Available online at www.sciencedirect.com

ScienceDirect

journal homepage: www.elsevier.com/locate/he

Shaggy-like Ru-clusters decorated core-shell metal-organic framework-derived CoO_x@NPC as high-efficiency catalyst for $NaBH_4$ hydrolysis

Shasha Dou [a], *Wanyu Zhang* [a], *Yuting Yang* [a], *Shuqing Zhou* [a], *Xianfa Rao* [b], *Puxuan Yan* [a], *Tayirjan Taylor Isimjan* [c,**], *Xiulin Yang* [a,*]

[a] *Guangxi Key Laboratory of Low Carbon Energy Materials, School of Chemistry and Pharmaceutical Sciences, Guangxi Normal University, Guilin, 541004, China*

[b] *School of Resources and Environmental Engineering, Jiangxi University of Science and Technology, Ganzhou, 341000, China*

[c] *Saudi Arabia Basic Industries Corporation (SABIC) at King Abdullah University of Science and Technology (KAUST), Thuwal, 23955-6900, Saudi Arabia*

HIGHLIGHTS

- Ru/CoO_x@NPC is fabricated by a seed-mediated growth plus precise calcination.
- The catalyst exhibits high activity and reusability for $NaBH_4$ hydrolysis.
- Carbonized ZIF-8 and ZIF-67 provide high conductivity and rich active sites.
- The superior performance attributed to the synergy of Co oxides and Ru clusters.

GRAPHICAL ABSTRACT

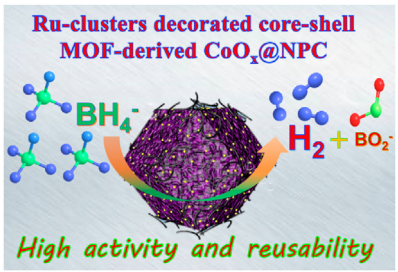

ARTICLE INFO

Article history:
Received 16 August 2020
Received in revised form
16 November 2020
Accepted 2 December 2020
Available online xxx

Keywords:
Metal-organic frameworks
N-doped porous carbon

ABSTRACT

Achieving high catalytic performance with the lowest possible amount of noble metal is critical for any catalytic applications. Herein, we report a controllable method of preparing low Ru loaded, N-doped porous carbon embedded with cobalt oxide species (Ru/CoO_x@-NPC) using core-shell metal-organic framework (MOF) as a template. The optimized catalyst exhibits a highly powerful yet stable performance of H_2 production through sodium borohydride ($NaBH_4$) hydrolysis. The Ru/CoO_x@NPC catalyst shows a fast H_2 generation rate (8019.5 mL min^{-1} g_{cat}^{-1}), high turnover frequency (1118.6 mol min^{-1} mol_{Ru}^{-1}), and reusability. The carbonized ZIF-8 core and the ZIF-67 outer shell supplies a porous carbon moiety that not only improves the conductivity and but also provides uniform distribution of the active sites. The XPS analysis indicates that there is a strong electronic interaction

* *Corresponding author.*
** *Corresponding author.*
E-mail addresses: isimjant@sabic.com (T.T. Isimjan), xlyang@gxnu.edu.cn (X. Yang).

https://doi.org/10.1016/j.ijhydene.2020.12.011

Please cite this article as: Dou S et al., Shaggy-like Ru-clusters decorated core-shell metal-organic framework-derived CoO_x@NPC as high-efficiency catalyst for $NaBH_4$ hydrolysis, International Journal of Hydrogen Energy, https://doi.org/10.1016/j.ijhydene.2020.12.011

Synergistic effect
$NaBH_4$ hydrolysis
Hydrogen generation

between Co species and Ru species. The superior catalytic performance can be attributable to the large specific surface area as well as the synergy between Co-oxide and Ru clusters.

Introduction

The growing demand for fossil fuels (*e.g.*, coal, oil and natural gas, *etc.*) is a significant cause of global warming resulted from accessed CO_2 emissions [1,2]. Therefore, developing a sustainable energy source and decreasing fossil fuel dependency is the central theme of clean energy research [3]. As an alternative energy carrier, hydrogen is becoming more and more viable due to its high energy density and zero CO_2 emission [4]. The two main challenges in developing H_2 fuel are the cost and safe-storage since the traditional H_2 storage involves high-energy requirements and complex technical issues. In general, the hydrogen storage methods for subsequent use can be divided into physical storage [5], such as pure hydrogen storage via compression and liquefaction, and chemical storage including metal hydride [6] and liquid organic hydrogen carriers [7], *etc.* As a chemical storage approach, the metal hydrides (*e.g.*, $NaBH_4$, $LiAlH_4$, MgH_2, *etc.*) have received more and more attention in recent years due to their safety, and adaptability to the mild reaction conditions [8,9]. Among them, sodium borohydride ($NaBH_4$) has the advantages of high hydrogen density, non-flammability, controllable hydrogen production rate, moderate operating temperature, excellent stability in alkaline solution, non-toxic hydrolysis by-products [10,11], *etc.* One of the widely believed challenges in using $NaBH_4$ as the hydrogen storage material is regeneration. However, recent studies have shown that $NaBH_4$ can be regenerated by high-energy ball milling of the hydrolysate in an argon atmosphere at room temperature. The yield can reach up to 80%, and it is scalable [12]. In addition, some other regeneration methods have reported regeneration rates ranging from 60% to 90% [13–15].

However, the spontaneous hydrolysis of $NaBH_4$ is a slow process thereof requires an efficient catalyst to decrease the activation energy and increase the reaction rate [16,17]. The commonly used catalysts are mainly noble metals, such as Pt/CeO_2–$Co_7Ni_2O_x$ [18], Pt–Co/carbon nanosphere [19], Pd/PD-ZIF-67 [20], Ag–Ni nanoparticles [21], Ru–Co catalysts [22], Ru/ZIF67 [23], *etc.* Same as other noble metal catalysts, they are limited by cost for industrial application [9]. As a result, many efforts have been devoted to developing Co-based none noble metal catalysts for $NaBH_4$ hydrolysis due to the high activity and low cost [14,24,25]. Nevertheless, they are suffered from rapid deactivation [26,27]. Recently, we reported a novel method of incorporating relatively small amounts of RuP_3 onto hierarchically structured cobalt phosphide arrays on nickel foam. This approach produced a highly efficient and stable catalyst for hydrogen generation from $NaBH_4$ hydrolysis in alkaline media [28].

As the continuation of this work, we aim to improve the catalytic performance further while decreasing the Ru loading. This goal can be realized by adjusting the support properties towards better conductivity and accelerated mass transfer. Recently, Pan et al. reported a high-performance nanostructured catalyst based on ZIF-67@ZIF-8 core-shell template [29]. Based on the results, they claim that the excellent catalytic performance is the outcome of the accelerated diffusion kinetics originated from the unique nanostructure [30]. Moreover, heteroatom N doping has been demonstrated that it can improve the surface wettability and create sufficient local reaction sites by changing the charge distribution on the carbon surface [31,32]. In light of their work, we have designed a novel catalyst of Ru-clusters loaded CoO_x@NPC using core-shell MOF template for $NaBH_4$ hydrolysis. This bifunctional catalyst was prepared in three steps, namely ZIF-67@ZIF-8 preparation, pyrolysis, and Ru loading. The catalytic test results reveal that the Ru/CoO_x@NPC catalyst has an outstanding H_2 generate rate, turnover frequency and durability, far better than these of all control catalysts.

Experimental section

Synthesis of ZIF-8 and nitrogen-doped porous carbon (NPC-8)

All chemicals used in this work are analytical grades and used directly without further purification. In a typical synthesis, we first prepared two stock solutions in methanol including, $Zn(NO_3)_2{\cdot}6H_2O$ (3 mmol, 30 mL) and 2-methylimidazole (2-MeIm, 12 mmol, 10 mL). Then, the 2-MeIm solution was added to a zinc nitrate solution and aged for 24 h at room temperature. The resulted white precipitate was collected by centrifugation, washed three times with methanol and vacuum-dried at 70 °C for 12 h. The obtained white powder was heated to 800 °C with a heating rate of 5 °C min^{-1} under Ar atmosphere and kept at 800 °C for 2 h. The collected sample was nominated as nitrogen-doped porous carbon (NPC-8).

Synthesis of ZIF-67 and CoO_x@N-doped carbon (CoO_x@NC-67)

Firstly, two stock solutions such as $Co(NO_3)_2{\cdot}6H_2O$ (1.6 g, 80 mL) and 2-MeIm (3.7 g, 80 mL) were prepared in methanol. Secondly, the solution of 2-MeIm was quickly poured into the solution of $Co(NO_3)_2{\cdot}6H_2O$ and then aged for 24 h at room temperature. The resulted white precipitate was collected by centrifugation, washed three times with abundant methanol

Please cite this article as: Dou S et al., Shaggy-like Ru-clusters decorated core-shell metal-organic framework-derived CoO_x@NPC as high-efficiency catalyst for $NaBH_4$ hydrolysis, International Journal of Hydrogen Energy, https://doi.org/10.1016/j.ijhydene.2020.12.011

and vacuum-dried at 70 °C for 12 h. Finally, the obtained purple powder (ZIF-67) was heated to 800 °C with a heating rate of 5 °C min^{-1} under Ar atmosphere and kept at 800 °C for 2 h. The resulted sample was named as CoO_x@nitrogen-doped carbon (CoO_x@NC-67, includes Co metal when x = 0).

Synthesis of ZIF-8@ZIF-67 and CoO_x@NPC composites

ZIF-8 (240 mg) was dispersed in 30 mL of methanol to form a homogeneous suspension after 30 min of sonication. A stock solution of $Co(NO_3)_2 \cdot 6H_2O$ (531 mg, 9 mL) and 2-MeIm (2.685 g, 9 mL) was added to the above suspension. Five minutes later, the obtained solution was transferred to an autoclave and kept at 100 °C for 12 h. After cooling to room temperature, the formed precipitate was centrifuged, washed with a large amount of methanol, and vacuum-dried at 70 °C for 12 h. The obtained purple precipitates are named as ZIF-8@ZIF-67. As a control, different molar ratios of Co/Zn precursors were used to synthesize a series of ZIF-8@ZIF-67. The ZIF-8@ZIF-67 composite was then heated to 800 °C with a heating rate of 5 °C min^{-1} under Ar atmosphere and kept at 800 °C for 2 h. The resulted sample was nominated as CoO_x@nitrogen-doped porous carbon (CoO_x@NPC). The content of C and N in the optimized material was analyzed by an element analyzer (Table S1), while Co and Zn were measured by ICP-AES (Table S2).

Synthesis of Ru/CoO_x@NPC composite

Typically, 30 mg CoO_x@NPC and different masses of $RuCl_3 \cdot 3H_2O$ were ultrasonically dispersed into 20 mL H_2O to form a homogeneous suspension. After continuous stirring for 5 h, 2 mL of 0.6 M $NaBH_4$ solution was added dropwise into the above mixture. Thirty minutes later, the resulted black precipitate was collected by centrifugation, washed three times with abundant water, and finally freeze-dried at 70 °C for 12 h to obtain the final product of Ru/CoO_x@NPC. The ICP-AES test results show that the mass percentage of Ru in the composite ranges from 1.69 wt% to 3.38 wt%, and the Ru mass percentage of 2.73 wt% has the best catalytic performance.

As a comparison, a mass percentage of 2.72 wt% Ru was applied to synthesize all other control catalysts. Notably, all the synthetic processes were as described above besides that the mass of the $RuCl_3 \cdot 3H_2O$ was fixed at 8.0 mg, and the support was replaced with NPC-8, CoO_x@NC-67, and XC-72 carbon black, respectively. The obtained catalysts were nominated as Ru/NPC-8, Ru/CoO_x@NC-67, and Ru/CB, respectively.

Catalyst characterizations

The crystal structure of catalysts was analyzed by X-ray powder diffraction (XRD, Rigaku D/Max 2500 V/PC) with a sweep speed for 2.0° min^{-1}. The morphologies and microstructures of the catalysts were characterized by scanning electron microscope (SEM, FEI Quanta 200 FEG) and transmission electron microscope (TEM, JEM-2100F). The X-ray photoelectron spectrometer (XPS, JPS-9010 Mg Kα) was used to analyze the chemical states of different elements. The specific surface area of the as-prepared product was measured on a Quantachrome Autosorb AS-1 instrument. The actual loadings of various metals in the catalyst were checked by inductively coupled plasma atomic emission spectroscopy (ICP-AES, IRIS Intrepid II XSP).

Catalytic hydrolysis for H_2 generation

The catalytic activity, cycle stability and activation energy of the catalytic materials were obtained by the following methods. First, 50 mL of 150 mM $NaBH_4$ (containing 0.4 wt% NaOH) was added to a three-necked round bottom flask (100 mL) and continuously stirred in a water bath at 25 °C for 0.5 h until the connected electronic balance stabilized to zero. Then, 10 mg of the catalyst was added to the above solution at 25 °C under continuous stirring. The generated H_2 was evaluated by drainage method, where the overflowed water was collected during the catalytic H_2 production process and the quality of the water was recorded in real-time via a computer-connected electronic balance. The hydrogen generation rate (HGR) and turnover frequency (TOF) can be obtained by converting the quality of the drainage water over time (see supplementary information) [33,34]. To test the catalyst's reusability, we measured the catalytic performance five times at 25 °C. After each reusability test, we centrifuged the catalyst, dried it under vacuum at room temperature, and obtained the catalyst's weight. All experiments were repeated three times to ensure reliable results. The activation energy of the designed catalyst was evaluated in the same device in the temperature range of 298–318 K.

Results and discussion

Synthetic strategy analysis

The schematic diagram of the preparation method of porous Ru/CoO_x@NPC composite is shown in Scheme 1. Step 1: the ZIF-8 was synthesized by a conventional manner, in which a mixture of zinc nitrate and 2-MeIm in methanol was aged at room temperature for 24 h [35]. Step 2: the ZIF-67 was grown onto the ZIF-8 surface to form ZIF-67@ZIF-8 composite through the hydrothermal method at 100 °C for 24 h [30,36]. Step 3: the ZIF-8@ZIF-67 composite was placed in a ceramic boat and carbonized at 800 °C to prepare the CoO_x@NPC composite. Step 4: the Ru clusters loading process was accomplished through direct chemical reduction of Ru^{3+} using $NaBH_4$ solution. The actual Ru loadings were determined by ICP-AES and the corresponding results were used to calculate the HGR and TOF values (Table S3). The rest of the controls were prepared in the similar manner. Moreover, a detailed investigation of the pyrolysis process of each intermediate using thermogravimetric (TG) analysis combined with mass spectrometry (MS) gives a useful insight of the pyrolysis mechanism (Fig. S1).

Crystallinity, microstructure and porosity analysis

Scanning electron microscopy (SEM) showed that the as-prepared ZIF-8 and ZIF-67 had a similar polyhedral morphology with an average particle size of 400 nm (Figs.

Please cite this article as: Dou S et al., Shaggy-like Ru-clusters decorated core-shell metal-organic framework-derived CoO_x@NPC as high-efficiency catalyst for $NaBH_4$ hydrolysis, International Journal of Hydrogen Energy, https://doi.org/10.1016/j.ijhydene.2020.12.011

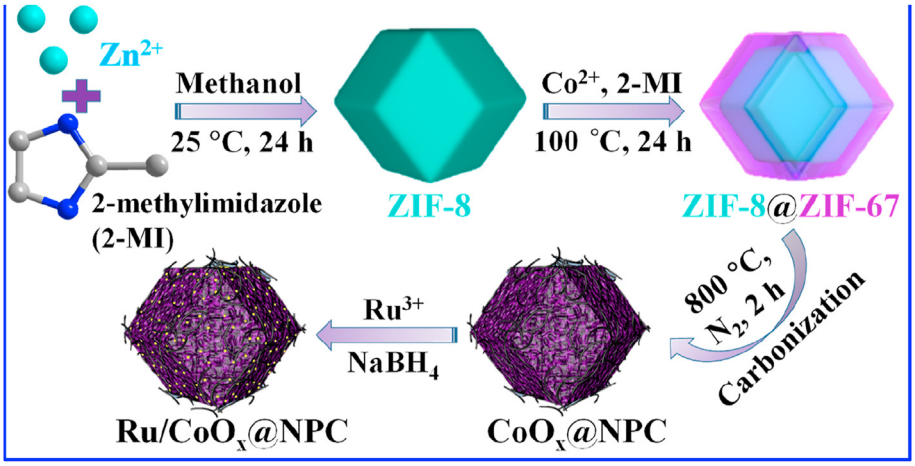

Scheme 1 – Schematic diagram of the synthesis of Ru/CoO_x@NPC composite.

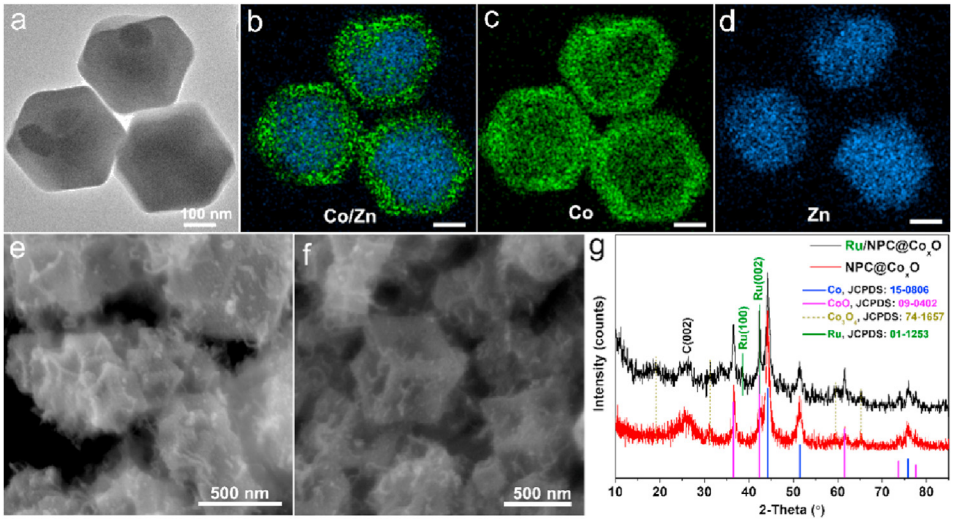

Fig. 1 – (a) TEM image of ZIF-8@ZIF-67 and (b–d) the corresponding elemental mappings of Zn and Co. SEM images of (e) CoO_x@NPC and (f) Ru/CoO_x@NPC composites. (g) XRD patterns of Ru/CoO_x@NPC and CoO_x@NPC.

S2a–b). The ZIF-67@ZIF-8 is about 500 nm in particle size (Fig. S2c), suggesting around 100 nm ZIF-67 grown on the ZIF-8. As shown in Fig. 1a, transmission electron microscopy (TEM) image shows that ZIF-8@ZIF-67 exhibits a clear edges and well-defined polyhedral structures, and the corresponding elemental distribution mappings further clearly demonstrate the existence of the core-shell structure (Fig. 1b–d). Upon carbonized at 800 °C for 2 h in Ar atmosphere, the polyhedral morphology of ZIF-8@ZIF-67 was partially inherited to the CoO_x@NPC (Fig. 1e). It is worth noting that a large number of carbon nanotubes penetrate through the structure of the collapsed polyhedron, and the surface is distributed with many particulate materials. After chemical reduction of the Ru clusters, we did not observe any notifiable changes in the microstructure, indicating that the deposition of Ru clusters on the surface of CoO_x@NPC does not affect in the overall morphology of CoO_x@NPC (Fig. 1f).

The X-ray diffraction (XRD) patterns of different calcination temperatures and Ru-clusters decorated different carriers are explored in detail in Fig. S3. Upon carbonizing at 800 °C in Ar atmosphere (Fig. 1g), the resulting CoO_x@NPC mainly exhibits the diffraction peaks belong to three Co species such as Co (JCPDS: 15–0806), CoO (JCPDS: 09–0402), and Co_3O_4 (JCPDS: 74–1657) [20,37]. After chemical deposition of Ru clusters, there are two additional diffraction peaks appeared at 38.6° and 42.4°, which are consistent with the characteristic peaks of hexagonal structure of metallic Ru (JCPDS: 01–1253) [38]. Moreover, X-ray diffraction (XRD) patterns of ZIF-8, ZIF-67 and core-shell ZIF-8@ZIF-67 are confirmed in Fig. S4a, and Raman spectra were adopted to investigate the effects of carbonization temperatures and support types on the carbon structure (Figs. S4b–c).

To further examine the microscopic features of Ru/CoO_x@NPC composite, we performed a detailed TEM study. Most of the black clusters (probably Co or Ru) are evenly distributed throughout the composite and some of which are agglomerated to a bigger particle (Fig. 2a). The high-resolution TEM image reveals that there are two types of distinct intersecting lattice fringes with the lattice spacing of 0.18 nm and 0.20 nm, and they are corresponding to the (111) and (200)

Please cite this article as: Dou S et al., Shaggy-like Ru-clusters decorated core-shell metal-organic framework-derived CoO_x@NPC as high-efficiency catalyst for $NaBH_4$ hydrolysis, International Journal of Hydrogen Energy, https://doi.org/10.1016/j.ijhydene.2020.12.011

planes of metallic Co (Fig. 2b) [39], respectively. Meanwhile, the lattice fringes with a spacing of 0.21 nm is ascribed to the (200) crystal plane of CoO [40], a lattice spacing of 0.34 nm is corresponding to the (002) crystal plane of graphitized carbon, and the other lattice spacing of 0.23 nm belongs to Ru (100) crystal plane [41]. Furthermore, the HAADF-STEM and corresponding elemental mappings indicate that the elements of Ru, Co, Zn, C, N and O are evenly distributed throughout the skeletal structure of Ru/CoO_x@NPC composite (Fig. 2c). Notably, since the particle size of Ru is so small that we can hardly distinguish Ru particles. Notably, the much sparser dispersion of Ru pattern is consistent with the features of ultralow loading of Ru species in the composite.

The N_2 adsorption/desorption isotherm at 77 K of Ru/CoO_x@NPC composite was used to investigate the Brunauer-Emmett-Teller (BET) surface area and porous structure (Fig. 2d). The BET curve shows a typical H3 type isotherm with a BET surface area of *ca.* 325.0 $m^2\ g^{-1}$ and a total pore volume of 0.206 $cm^2\ g^{-1}$. The isotherm shows a rapid increase at a lower relative pressure ($P/P_0 < 0.02$), indicating the presence of a mesoporous structure. Notably, there is a distinct hysteresis loop at relative pressures (P/P_0) of 0.5–0.9, which are mainly originated from the structural voids of the surface collapse of the composite [42]. Moreover, the porous size distribution of the composite is in the range of 0.73–2.7 nm from the Barrett-Joyner-Halenda (BJH) analysis showing the micropores and mesopores porous mixed features. The high porosity exposes more active sites, and facilitates the diffusion of solutes and the release of gases, therefore improves the catalytic performance.

XPS analysis

The compositions and chemical states of Ru/CoO_x@NPC and CoO_x@NPC were studied by X-ray photoelectron spectroscopy (XPS). As shown in Fig. S5a, the elements of C, N, O, and Co are detected in both samples by XPS survey spectra. The high-resolution XPS spectra of C 1s + Ru 3d regions (Fig. 3a) are deconvoluted into C=C (284.0 eV), C–C (284.8 eV) and C–O (286.1 eV) and used as a calibration standard [43,44]. Meanwhile, the Ru $3d_{5/2}$ core level from Ru clusters are deconvoluted at the binding energies of 281.0 eV (Ru^0) and 283.2 eV (Unscreened final states) [45]. Fig. 3b shows the high-resolution Co 2p spectra of Ru/CoO_x@NPC and CoO_x@NPC, where the Co $2p_{3/2}$ region of Ru/CoO_x@NPC is deconvoluted into three peaks at 778.5, 780.6 and 784.6 eV, corresponding to the metallic Co, Co^{2+} and satellite peaks, respectively. Compared with CoO_x@NPC, the Co^{2+} species in Ru/CoO_x@NPC undergoes a positive shift (0.93 eV), which is smaller than that of the binding energy differences of Co $2p_{1/2}$ of Co^{2+} and Co^{3+} (1.2 eV) [46], indicating a strong electronic interaction between Ru and Co species [47]. Notably, the peak ratios of Co^{2+}/Co increased from 7.6 to 15.2 after the Ru loading on the CoO_x@NPC surface, which could be due to the oxidation of the surface of CoO_x@NPC. Moreover, the high-resolution O 1s spectra of the two samples are further analyzed (Fig. 3c). The resulting three type of signals at 529.5, 530.8 and 532.1 eV are ascribed to metal oxide, oxygen vacancies and adsorbed H_2O, respectively [48]. As shown in Fig. 3c, the oxygen vacancies ratio increase rapidly from 42.6% to 67.9% after Ru loading. Many studies have found that a higher proportion of oxygen vacancies creates a faster electron transfer, stronger adsorption characteristics and more active sites [49]. Furthermore, it

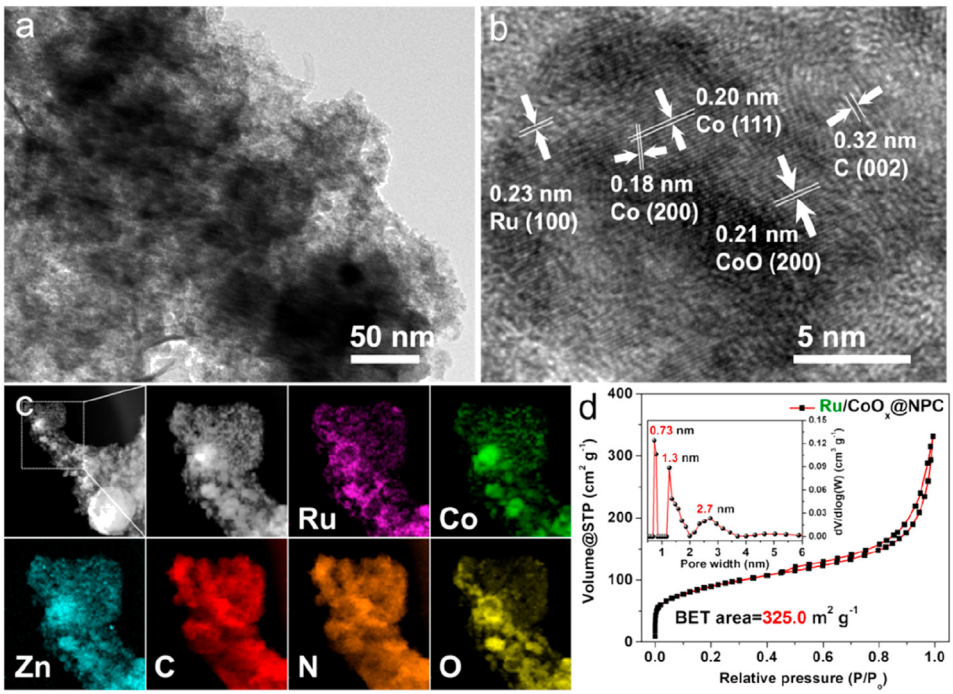

Fig. 2 – (a) TEM and (b) high-resolution TEM images of Ru/CoO_x@NPC. (c) HAADF-STEM image of Ru/CoO_x@NPC, and the corresponding element mappings of Ru, Co, Zn, C, N and O. (d) N_2 adsorption–desorption isotherms with pore-size distributions by the BJH method of Ru/CoO_x@NPC.

Please cite this article as: Dou S et al., Shaggy-like Ru-clusters decorated core-shell metal-organic framework-derived CoO_x@NPC as high-efficiency catalyst for $NaBH_4$ hydrolysis, International Journal of Hydrogen Energy, https://doi.org/10.1016/j.ijhydene.2020.12.011

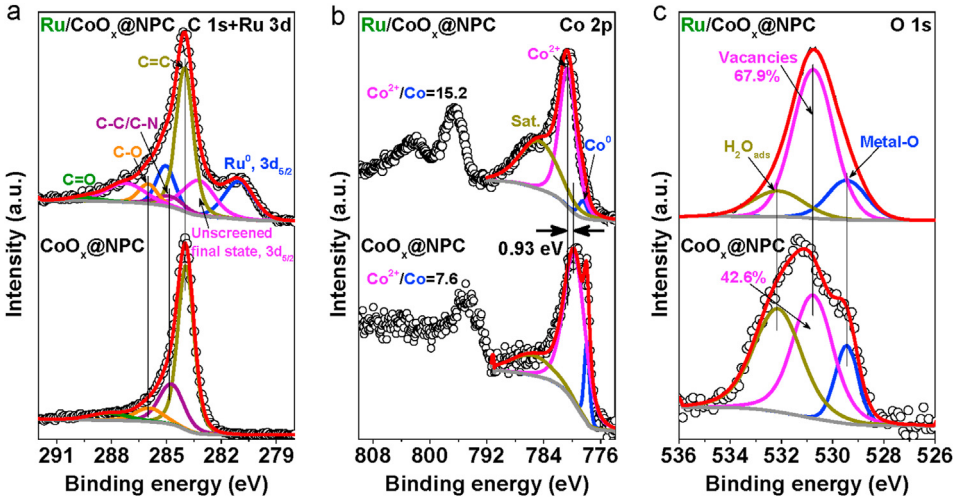

Fig. 3 – High-resolution XPS spectra of (a) C 1s + Ru 3d, (b) Co 2p and (c) O 1s regions from Ru/CoO$_x$@NPC and CoO$_x$@NPC.

should be pointed that the high-resolution N 1s spectra did not change much before and after loading of Ru clusters (Figs. S5b–c), further demonstrating that the loading process of Ru does not destroy the composition of the material [50].

Catalytic hydrolysis analysis

The catalytic H_2 production from $NaBH_4$ hydrolysis were performed in an alkalized $NaBH_4$ solution at 25 °C. The schematic illustration of the experimental setup is shown in Fig. S6. The amounts of the generated H_2 was calculated according to the volume of the water displaced by H_2. The self-hydrolysis study of $NaBH_4$ was first carried out in 150 mM $NaBH_4$ + 0.4 wt% NaOH solution, and almost no hydrogen evolution was detected (Fig. S7). As shown in Fig. 4a, we explored the effect of the carbonization temperature of Ru/CoO$_x$@NPC on catalytic performance. The higher annealing temperature changes the catalyst's crystallinity, thereby improving catalytic performance; meanwhile, it also decreases the catalyst's porosity. Therefore, the optimal point is expected. The results show that the optimized Ru/CoO$_x$@NPC catalyst prepared by carbonized at 800 °C has the highest turnover frequency (TOF) of 1118.6 mol_{H2} mol_{Ru}^{-1} min^{-1} among the rest (Fig. 4b). This is one of the highest reported value of Ru

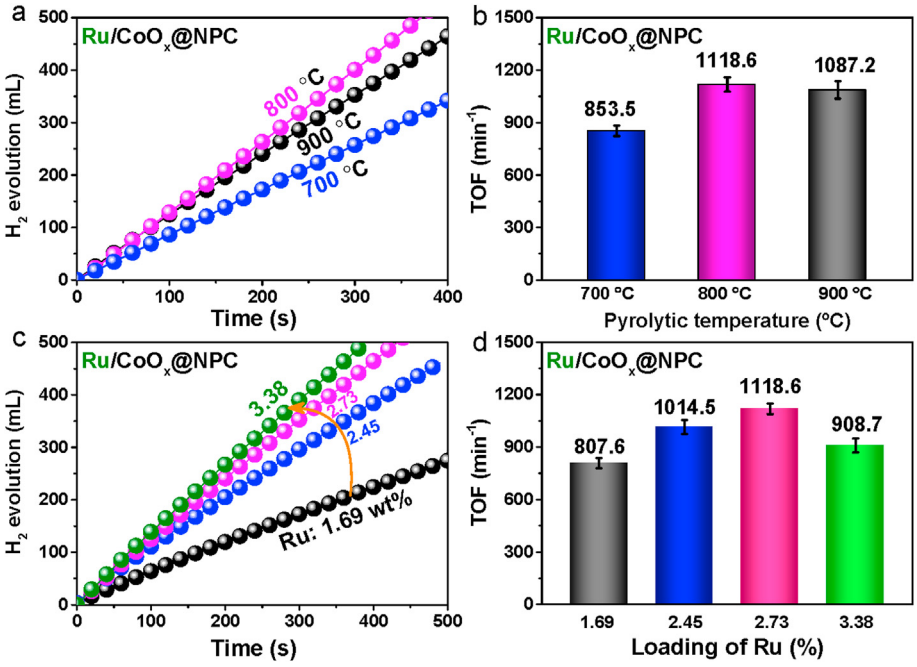

Fig. 4 – (a) Stoichiometric H_2 evolution and (b) the summarized TOF values by Ru/CoO$_x$@NPC catalysts with different pyrolysis temperatures at 25 °C. (c) The relationship between the H_2 generation rates and loadings of Ru species on Ru/CoO$_x$@NPC catalysts, and (d) the summarized TOF values. All the experiment are conducted in 150 mM $NaBH_4$ + 0.4 wt % NaOH solution at 25 °C.

Please cite this article as: Dou S et al., Shaggy-like Ru-clusters decorated core-shell metal-organic framework-derived CoO$_x$@NPC as high-efficiency catalyst for $NaBH_4$ hydrolysis, International Journal of Hydrogen Energy, https://doi.org/10.1016/j.ijhydene.2020.12.011

loaded powder catalysts for $NaBH_4$ hydrolysis (Table S4) to the best of our knowledge. In addition, we optimize the loading of Ru in terms of catalytic performance. The results show that as the contents of Ru increases, the catalytic hydrogen generation increases rapidly at the beginning and then slows down when it close to the maximum point around 3.0 wt% (Fig. 4c). The catalyst has the largest TOF value when the Ru loading is 2.73 wt% (Fig. 4d). The results revealed that the Ru/CoO_x@NPC prepared by the precursor with Co/Zn ratio of 3/4 shows the best catalytic performance (Fig. S8). The equivalent H_2 per mole of $NaBH_4$ was used in the vertical axis to signify the changes in conversion (Figs. S9a–b). Therefore, the Ru loading in the Ru/CoO_x@NPC catalyst discussed below is 2.73 wt%, and CoO_x@NPC is prepared by carbonization at 800 °C in Ar atmosphere.

To evaluate the effect of different supports on the catalytic performance, we investigated the catalytic performance on various supports with the same loading of Ru (2.73 wt%). As shown in Fig. 5a and Fig. S9c, the catalytic activity of Ru loaded CoO_x@NPC was found to be substantially higher than that of CoO_x@NPC as well as all other control catalysts. Fig. 5b shows that the HGR values of Ru/CoO_x@NPC is 8019.5 mL min^{-1} g_{cat}^{-1} (total mass of catalyst), which is 1.44–, 4.57–, 716.0– and 47.53–fold higher than that of Ru/CoO_x@NC-67, Ru/CB, Ru/NPC-8 and NPC-67 respectively, while also superior to most of the previously reported catalysts (Table S4). In particular, the metal ICP-AES test results show that the content of Zn in the target catalyst is very low, and the actual content is between 1% and 3%. In combination with Fig. 5a, the catalytic performance of Ru/NPC-8 is very weak, indicating that Zn has little effect on the performance of catalyzing hydrogen evolution as an impurity. To measure the activation energies of Ru/CoO_x@NPC and Ru/CoO_x@NC-67, a set of experiments were conducted at different temperatures. As shown in Fig. 5c and Fig. S9d, the rate of HGR values increase rapidly with increasing the reaction temperatures from 298 K to 318 K, and the rate constant κ is calculated from the slope of each experiment. The activation energy of Ru/CoO_x@NPC catalyst was estimated to be 54.2 kJ mol^{-1} by the Arrhenius plot (ln κ vs 1/T), which is lower than that of Ru/CoO_x@NPC (59.3 kJ mol^{-1}) (Fig. 5d and Fig. S10), implying a kinetically enhanced catalytic activity towards $NaBH_4$ hydrolysis [51].

Durability tests are used to evaluate the reusability of Ru/CoO_x@NPC catalyst in an alkalized $NaBH_4$ solution (Fig. 6a). The results show that the Ru/CoO_x@NPC catalyst exhibits excellent reusability for catalytic hydrogen generation. After the fifth cycle, it retained *ca.* 73.9% of initial activity (Fig. 6b). The slight decay of catalytic activity could be attributed to the exfoliation of Ru species (the mass fraction of Ru species is reduced from 2.73% to 2.10% by ICP-AES after five recycles, Table S3), structural damage (Fig. S11) and catalyst poisoning by BO_2^- species [28,52].

As discussed above, the Ru/NPC@CoO_x catalyst has the largest HGR and TOF values as compare to other catalysts. The outstanding performance mainly attributed to a large specific surface area, high conductivity, and synergy between Co and Ru species. According to the XPS study, the positive shift of the Co 2p binding energy in Ru/CoO_x@NPC caused by the partial electron transfer from Co species to Ru species indicates a higher electron density on Co species as compared to that of Ru species. Accordingly, the partially negatively charged hydrogen atoms preferred to attach to the Ru atoms. As a result, the BH_4^- dissociates at the Co and Ru metal sites, on which hydrogen atoms are adsorbed on Ru and BH_3 is

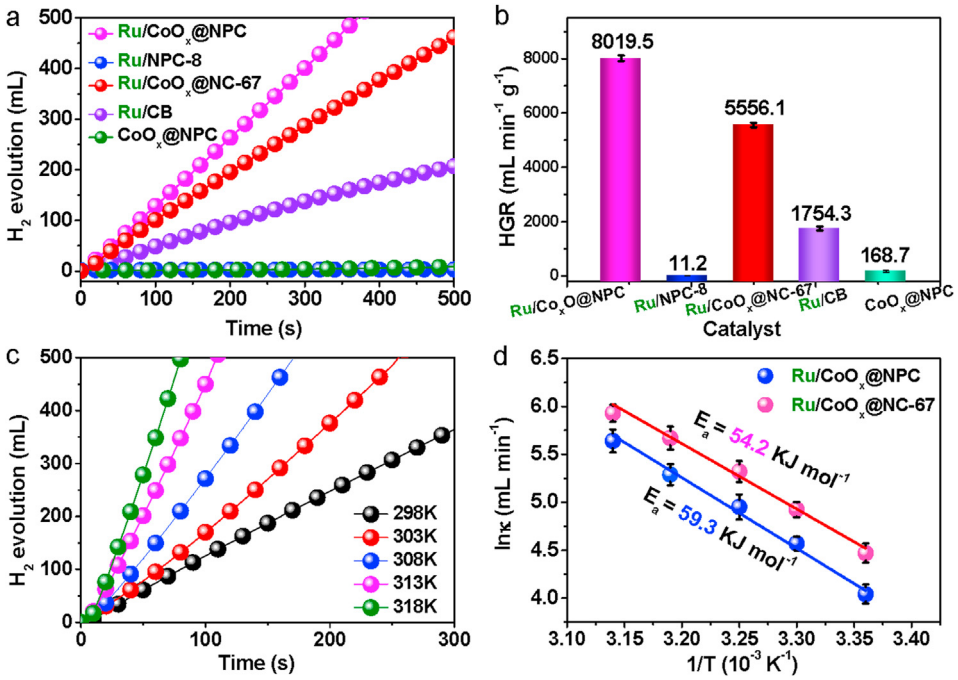

Fig. 5 – (a) Stoichiometric H_2 evolution and (b) the summarized TOF values of different catalysts (2.73 wt% Ru) in 150 mM $NaBH_4$ + 0.4 wt% NaOH solution at 25 °C. (c) Stoichiometric H_2 evolution of Ru/CoO_x@NPC in 150 mM $NaBH_4$ + 0.4 wt% NaOH solution at different reaction temperatures, and (d) the summarized Arrhenius plots from c.

Please cite this article as: Dou S et al., Shaggy-like Ru-clusters decorated core-shell metal-organic framework-derived CoO_x@NPC as high-efficiency catalyst for $NaBH_4$ hydrolysis, International Journal of Hydrogen Energy, https://doi.org/10.1016/j.ijhydene.2020.12.011

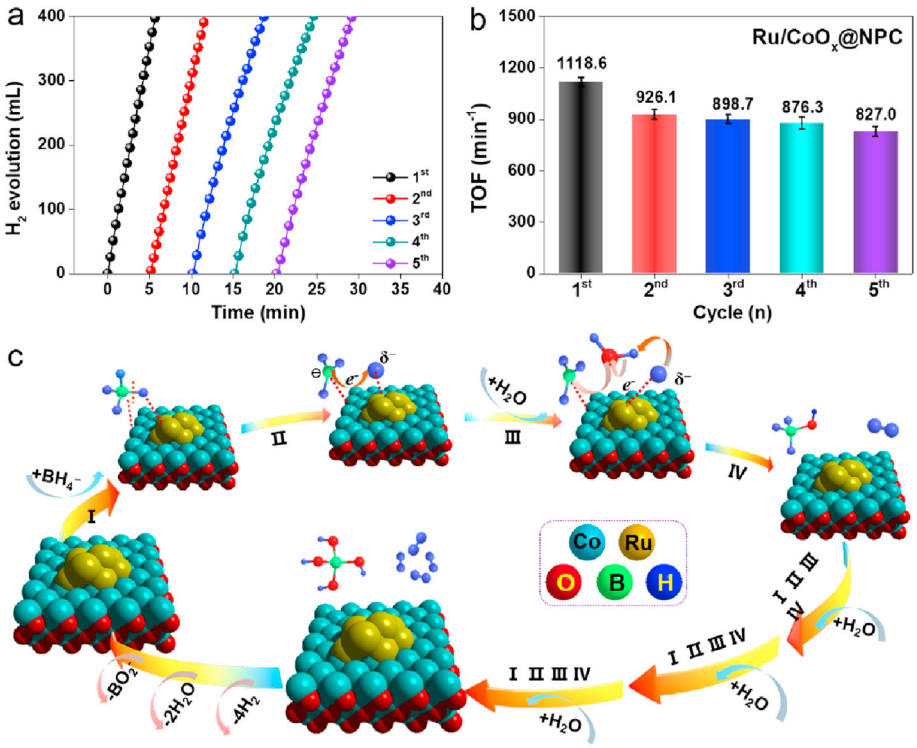

Fig. 6 – (a) Reusability test of Ru/CoO_x@NPC catalyst in 150 mM $NaBH_4$ + 0.4 wt % NaOH at 25 °C. (b) The summarized TOF values in different reusability test. (c) The proposed catalytic mechanism of Ru/CoO_x@NPC catalyst for H_2 generation.

attached to Co species. After the B–H bond is broken, the negatively charged B species immediately transfers the negative charge to the adsorbed H atoms through the conductive bulk. Finally, the negatively charged H atom on the Ru surface extracts hydrogen from water to release an H_2 molecule, while the OH^- ion attacks the BH_3 to form a BH_3OH molecule, followed by transferring one hydrogen atom of the BH_3OH to a free Ru site. After the first cycle, the surface of the catalyst releases a hydrogen molecule and a BH_3OH species. As the reaction proceeds, all of the H atoms in the borohydride are replaced by OH^- ions (Fig. 6c), ultimately releasing the $B(OH)_4^-$ species [53].

Conclusion

In summary, core-shell ZIF-8@ZIF-67 crystals, which integrate the properties of single ZIF-8 and ZIF-67, are elaborately designed and fabricated using a seed-mediated growth technique. Upon the direct carbonization of core-shell ZIF-8@ZIF-67 crystals, a novel CoO_x@NPC supports are generated. The functionalized support inherent the high surface area (up to 325.0 $m^2\ g^{-1}$) derived from core ZIF-8 and superior graphitic structure originated from shell ZIF-67. Finally, the low-loading Ru decorated CoO_x@NPC was prepared through chemical reduction. The carbonization temperatures, types of supports, and loading contents of Ru clusters were studied in detail. The optimal performance on $NaBH_4$ hydrolysis was achieved under the condition where the pyrolysis temperature is 800 °C, and the Ru loading is 2.37 wt%. The highest TOF value of Ru/CoO_x@NPC catalyst is 1118.6 min^{-1} at 25 °C, far better than most previously reported results. Besides, the Ru/CoO_x@NPC catalyst still retains more than 70% catalytic activity after five cycles. This work provides new insight into designing and preparing a highly active catalyst for $NaBH_4$ hydrolysis.

Declaration of competing interest

The authors declare that they have no known competing financial interests or personal relationships that could have appeared to influence the work reported in this paper.

Acknowledgements

This work has been supported by the National Natural Science Foundation of China (no. 21965005), Natural Science Foundation of Guangxi Province (2018GXNSFAA294077, 2018GXNSFAA281220), Project of High-Level Talents of Guangxi (F-KA18015, 2018ZD004) and Guangxi Technology Base and Talent Subject (GUIKE AD18126001).

Appendix A. Supplementary data

Supplementary data to this article can be found online at https://doi.org/10.1016/j.ijhydene.2020.12.011.

Please cite this article as: Dou S et al., Shaggy-like Ru-clusters decorated core-shell metal-organic framework-derived CoO_x@NPC as high-efficiency catalyst for $NaBH_4$ hydrolysis, International Journal of Hydrogen Energy, https://doi.org/10.1016/j.ijhydene.2020.12.011

REFERENCES

[1] Lu XF, Yu L, Lou XW. Highly crystalline Ni-doped FeP/carbon hollow nanorods as all-pH efficient and durable hydrogen evolving electrocatalysts. Sci. Adv 2019;5:eaav6009.
[2] Huang LB, Zhao L, Zhang Y, Chen YY, Zhang QH, Luo H, Zhang X, Tang T, Gu L, Hu JS. Self-limited on-site conversion of MoO_3 nanodots into vertically aligned ultrasmall monolayer MoS_2 for efficient hydrogen evolution. Adv. Energy Mater. 2018;8:1800734.
[3] Tang C, Zhang R, Lu W, He L, Jiang X, Asiri AM, Sun X. Fe-doped CoP nanoarray: a monolithic multifunctional catalyst for highly efficient hydrogen generation. Adv Mater 2017;29:1602441.
[4] Ghodke NP, Rayaprol S, Bhoraskar SV, Mathe VL. Catalytic hydrolysis of sodium borohydride solution for hydrogen production using thermal plasma synthesized nickel nanoparticles. Int J Hydrogen Energy 2020;45:16591–605.
[5] Eberle U, Müller B, von Helmolt R. Fuel cell electric vehicles and hydrogen infrastructure: status 2012. Energy Environ Sci 2012;5:8780–98.
[6] Schneemann A, White JL, Kang S, Jeong S, Wan LF, Cho ES, Heo TW, Prendergast D, Urban JJ, Wood BC, Allendorf MD, Stavila V. Nanostructured metal hydrides for hydrogen storage. Chem Rev 2018;118:10775–839.
[7] Aakko-Saksa PT, Cook C, Kiviaho J, Repo T. Liquid organic hydrogen carriers for transportation and storing of renewable energy – review and discussion. J Power Sources 2018;396:803–23.
[8] Yao Q, Lu Z-H, Huang W, Chen X, Zhu J. High Pt-like activity of the Ni–Mo/graphene catalyst for hydrogen evolution from hydrolysis of ammonia borane. J Mater Chem A 2016;4:8579–83.
[9] Mori K, Miyawaki K, Yamashita H. Ru and Ru–Ni nanoparticles on TiO_2 support as extremely active catalysts for hydrogen production from ammonia–borane. ACS Catal 2016;6:3128–35.
[10] Yuan H, Huo W, Hao Y, Wang Y, Qiao W, Wang T, Zhu X. Hydrogen generation from hydrolysis of sodium borohydride using nanosized NiB amorphous alloy catalysts. Nano 2020;15:2050081.
[11] Uzundurukan A, Devrim Y. Hydrogen generation from sodium borohydride hydrolysis by multi-walled carbon nanotube supported platinum catalyst: a kinetic study. Int J Hydrogen Energy 2019;44:17586–94.
[12] Zhu Y, Ouyang L, Zhong H, Liu J, Wang H, Shao H, Huang Z, Zhu M. Closing the loop for hydrogen storage: facile regeneration of NaBH4 from its hydrolytic product. Angew Chem Int Ed 2020;59:8623–9.
[13] Ouyang L, Chen W, Liu J, Felderhoff M, Wang H, Zhu M. Enhancing the regeneration process of consumed $NaBH_4$ for hydrogen storage. Adv. Energy Mater. 2017;7:1700299.
[14] Zhang X, Zhang Q, Xu B, Liu X, Zhang K, Fan G, Jiang W. Efficient hydrogen generation from the $NaBH_4$ hydrolysis by cobalt-based catalysts: positive roles of sulfur-containing salts. ACS Appl Mater Interfaces 2020;12:9376–86.
[15] Zhong H, Ouyang L, Zeng M, Liu J, Wang H, Shao H, Felderhoff M, Zhu M. Realizing facile regeneration of spent $NaBH_4$ with Mg–Al alloy. J Mater Chem A 2019;7:10723–8.
[16] Liu J, Wang H, Yuan Q, Song X. A novel material of nanoporous magnesium for hydrogen generation with salt water. J Power Sources 2018;395:8–15.
[17] Abdelhamid HN. Hierarchical porous ZIF-8 for hydrogen production via the hydrolysis of sodium borohydride. Dalton Trans 2020;49:4416–24.
[18] Wu C, Zhang J, Guo J, Sun L, Ming J, Dong H, Zhao Y, Tian J, Yang X. Ceria-induced strategy to tailor Pt atomic clusters on cobalt–nickel oxide and the synergetic effect for superior hydrogen generation. ACS Sustainable Chem Eng 2018;6:7451–7.
[19] Zhang H, Zhang L, Rodríguez-Pérez IA, Miao W, Chen K, Wang W, Li Y, Han S. Carbon nanospheres supported bimetallic Pt-Co as an efficient catalyst for $NaBH_4$ hydrolysis. Appl Surf Sci 2021;540:148296.
[20] Wu C, Guo J, Zhang J, Zhao Y, Tian J, Isimjan TT, Yang X. Palladium nanoclusters decorated partially decomposed porous ZIF-67 polyhedron with ultrahigh catalytic activity and stability on hydrogen generation. Renew Energy 2019;136:1064–70.
[21] Al-Thabaiti SA, Khan Z, Malik MA. Bimetallic Ag-Ni nanoparticles as an effective catalyst for hydrogen generation from hydrolysis of sodium borohydride. Int J Hydrogen Energy 2019;44:16452–66.
[22] R F, S S, AM V. Carbon supported bimetallic Ru-Co catalysts for H_2 production through $NaBH_4$ and NH_3BH_3 hydrolysis. Int J Energy Res 2018;42:1183–95.
[23] Tuan DD, Lin K-YA. Ruthenium supported on ZIF-67 as an enhanced catalyst for hydrogen generation from hydrolysis of sodium borohydride. Chem Eng J 2018;351:48–55.
[24] Wei Y, Wang M, Fu W, Wei L, Zhao X, Zhou X, Ni M, Wang H. Highly active and durable catalyst for hydrogen generation by the $NaBH_4$ hydrolysis reaction: CoWB/NF nanodendrite with an acicular array structure. J Alloys Compd 2020;836:155429.
[25] Kim C, Lee SS, Li W, Fortner JD. Towards optimizing cobalt based metal oxide nanocrystals for hydrogen generation via $NaBH_4$ hydrolysis. Appl Catal A Gen 2020;589:117303.
[26] Akdim O, Demirci UB, Miele P. Deactivation and reactivation of cobalt in hydrolysis of sodium borohydride. Int J Hydrogen Energy 2011;36:13669–75.
[27] Xu J, Du X, Wei Q, Huang Y. Efficient hydrolysis of sodium borohydride by Co-B supported on nitrogen-doped carbon. Chemistry 2020;5:6683–90.
[28] Guo J, Wu C, Zhang J, Yan P, Tian J, Shen X, Isimjan TT, Yang X. Hierarchically structured rugae-like RuP_3–CoP arrays as robust catalysts synergistically promoting hydrogen generation. J Mater Chem A 2019;7:8865–72.
[29] Pan Y, Sun K, Liu S, Cao X, Wu K, Cheong WC, Chen Z, Wang Y, Li Y, Liu Y, Wang D, Peng Q, Chen C, Li Y. Core-shell ZIF-8@zif-67-derived CoP nanoparticle-embedded N-doped carbon nanotube hollow polyhedron for efficient overall water splitting. J Am Chem Soc 2018;140:2610–8.
[30] Tang J, Salunkhe RR, Liu J, Torad NL, Imura M, Furukawa S, Yamauchi Y. Thermal conversion of core-shell metal-organic frameworks: a new method for selectively functionalized nanoporous hybrid carbon. J Am Chem Soc 2015;137:1572–80.
[31] Deng LYD, Chen X, Wang G, Jin L, Pan X, Deng J, Sun G, Bao X. Iron encapsulated within pod-like carbon nanotubes for oxygen reduction reaction. Angew Chem, Int Ed 2013;572:371.
[32] Guo RSD, Akiba C, Saji S, Kondo T, Nakamura J. Active sites of nitrogen-doped carbon materials for oxygen reduction reaction clarified using model catalysts. Science 2016;351:361.
[33] Cui L, Xu Y, Niu L, Yang W, Liu J. Monolithically integrated CoP nanowire array: an on/off switch for effective on-demand hydrogen generation via hydrolysis of $NaBH_4$ and NH_3BH_3. Nano Res 2017;10:595–604.
[34] Yao Q, Lu Z-H, Yang Y, Chen Y, Chen X, Jiang H-L. Facile synthesis of graphene-supported Ni-CeO_x nano-composites as highly efficient catalysts for hydrolytic dehydrogenation of ammonia borane. Nano Res 2018;11:4412–22.
[35] Wang Z, Lu Y, Yan Y, Larissa TYP, Zhang X, Wuu D, Zhang H, Yang Y, Wang X. Core-shell carbon materials derived from

Please cite this article as: Dou S et al., Shaggy-like Ru-clusters decorated core-shell metal-organic framework-derived CoO_x@NPC as high-efficiency catalyst for $NaBH_4$ hydrolysis, International Journal of Hydrogen Energy, https://doi.org/10.1016/j.ijhydene.2020.12.011

metal-organic frameworks as an efficient oxygen bifunctional electrocatalyst. Nano Energy 2016;30:368–78.
[36] Liu S, Wang Z, Zhou S, Yu F, Yu M, Chiang C-Y, Zhou W, Zhao J, Qiu J. Metal–organic-framework-derived hybrid carbon nanocages as a bifunctional electrocatalyst for oxygen reduction and evolution. Adv Mater 2017;29:1700874.
[37] Tang C, Surkus A-E, Chen F, Pohl M-M, Agostini G, Schneider M, Junge H, Beller M. A stable nano-cobalt catalyst for selective dehydrogenation of formic acid with highly dispersed CoNx active sites. Angew Chem Int Ed 2017;56:16616–20.
[38] Joo SH, Park JY, Renzas JR, Butcher DR, Huang W, Somorjai GA. Size effect of ruthenium nanoparticles in catalytic carbon monoxide oxidation. Nano Lett 2010;10:2709–13.
[39] Ma X, Zhao X, Huang J, Sun L, Li Q, Yang X. Fine Co nanoparticles encapsulated in a N-doped porous carbon matrix with superficial N-doped porous carbon nanofibers for efficient oxygen reduction. ACS Appl Mater Interfaces 2017;9:21747–55.
[40] Tong Y, Chen P, Zhou T, Xu K, Chu W, Wu C, Xie Y. A bifunctional hybrid electrocatalyst for oxygen reduction and evolution: cobalt oxide nanoparticles strongly coupled to B,N-decorated graphene. AngewChem IntEd 2017;56:1–6.
[41] Li Y, Zhang LA, Qin Y, Chu F, Kong Y, Tao Y, Li Y, Bu Y, Ding D, Liu M. Crystallinity dependence of ruthenium nanocatalyst toward hydrogen evolution reaction. ACS Catal 2018;8:5714–20.
[42] Yang X, Wang X, Feng Y, Zhang G, Wang T, Song W, Shu C, Jiang L, Wang C. Removal of multifold heavy metal contaminations in drinking water by porous magnetic Fe_2O_3@AlO(OH) superstructure. J Mater Chem A 2013;1:473–7.
[43] Guo J, Wang B, Yang D, Wan Z, Yan P, Tian J, Isimjan TT, Yang X. Rugae-like Ni_2P-CoP nanoarrays as a bi-functional catalyst for hydrogen generation: $NaBH_4$ hydrolysis and water reduction. Appl Catal B: Environ 2020;265:118584.
[44] Qian M, Xu M, Zhou S, Tian J, Taylor Isimjan T, Shi Z, Yang X. Template synthesis of two-dimensional ternary nickel-cobalt-nitrogen co-doped porous carbon film: promoting the conductivity and more active sites for oxygen reduction. J Colloid Interface Sci 2020;564:276–85.
[45] Novio F, Philippot K, Chaudret B. Location and dynamics of CO Co-ordination on Ru nanoparticles: a solid state NMR study. Catal Lett 2010;140:1–7.
[46] Zhang R, Lu Y, Wei L, Fang Z, Lu C, Ni Y, Xu Z, Tao S, Li P. Synthesis and conductivity properties of $Gd_{0.8}Ca_{0.2}BaCo_2O_{5+\delta}$ double perovskite by sol–gel combustion. J Mater Sci-Mater Electron 2015;26:9941–8.
[47] Wang X, Chen L, Chong SY, Little MA, Wu Y, Zhu W-H, Clowes R, Yan Y, Zwijnenburg MA, Sprick RS, Cooper AI. Sulfone-containing covalent organic frameworks for photocatalytic hydrogen evolution from water. Nat Chem 2018;10:1180–9.
[48] Sun J, Guo N, Shao Z, Huang K, Li Y, He F, Wang Q. A facile strategy to construct amorphous spinel-based electrocatalysts with massive oxygen vacancies using ionic liquid dopant. Adv. Energy Mater 2018;8:1870121.
[49] Tong Y, Chen P, Zhang M, Zhou T, Zhang L, Chu W, Wu C, Xie Y. Oxygen vacancies confined in nickel molybdenum oxide porous nanosheets for promoted electrocatalytic urea oxidation. ACS Catal 2018;8:1–7.
[50] Peng X, Chen D, Yang X, Wang D, Li M, Tseng C-C, Panneerselvam R, Wang X, Hu W, Tian J, Zhao Y. Microwave-assisted synthesis of highly dispersed PtCu nanoparticles on three-dimensional nitrogen-doped graphene networks with remarkably enhanced methanol electrooxidation. ACS Appl Mater Interfaces 2016;8:33673–80.
[51] Kılınç D, Şahin Ö, Saka C. Salicylaldimine-Ni complex supported on Al_2O_3: highly efficient catalyst for hydrogen production from hydrolysis of sodium borohydride. Int J Hydrogen Energy 2018;43:251–61.
[52] Zhou L, Meng J, Li P, Tao Z, Mai L, Chen J. Ultrasmall cobalt nanoparticles supported on nitrogen-doped porous carbon nanowires for hydrogen evolution from ammonia borane. Mater. Horiz. 2017;4:268–73.
[53] Demirci UB, Miele P. Reaction mechanisms of the hydrolysis of sodium borohydride: a discussion focusing on cobalt-based catalysts. C. R. Chim 2014;17:707–16.

Please cite this article as: Dou S et al., Shaggy-like Ru-clusters decorated core-shell metal-organic framework-derived CoO_x@NPC as high-efficiency catalyst for $NaBH_4$ hydrolysis, International Journal of Hydrogen Energy, https://doi.org/10.1016/j.ijhydene.2020.12.011